Additive Manufacturing 16 (2017) 24–29

Contents lists available at ScienceDirect

Additive Manufacturing

journal homepage: www.elsevier.com/locate/addma

Compressive failure modes and energy absorption in additively manufactured double gyroid lattices

I. Maskery*, N.T. Aboulkhair, A.O. Aremu, C.J. Tuck, I.A. Ashcroft

Centre for Additive Manufacturing, Faculty of Engineering, University of Nottingham, Nottingham NG7 2RD, UK

ARTICLE INFO

Article history:
Received 17 March 2017
Received in revised form 25 April 2017
Accepted 30 April 2017

Keywords:
Additive manufacturing
Lattice
Gyroid
Selective laser melting

ABSTRACT

Lattice structures are excellent candidates for lightweight, energy absorbing applications such as personal protective equipment. In this paper we explore several important aspects of lattice design and production by metal additive manufacturing, including the choice of cell size and the application of a post-manufacture heat treatment. Key results include the characterisation of several failure modes in double gyroid lattices made of Al-Si10-Mg, the elimination of brittle fracture and low-strain failure by the application of a heat treatment, and the calculation of specific energy absorption under compressive deformation (16×10^6 J m^{-3} up to 50% strain). These results demonstrate the suitability of double gyroid lattices for energy absorbing applications, and will enable the design and manufacture of more efficient lightweight parts in the future.

1. Introduction

Additive manufacturing (AM) describes a range of processes that fabricate components directly from CAD representations in a sequence of bonded or integrated layers. AM components need not be constrained by the same design restrictions that apply to conventional manufacturing (e.g. subtraction or forming); they may be freeform and quite complex, providing the opportunity for lightweighting and increased functionality.

One way in which AM component redesign may be achieved is by the replacement of otherwise solid volumes with lightweight cellular structures, or lattices [1–7]. In terms of specific mechanical properties, latticed components may actually be sub-optimum compared to those stemming from topology optimisation (TO) approaches, but they may offer superior performance in cases which feature uncertainty in the loading conditions. Also, because they generally do not require the large computational resources associated with iterative TO, they are easier to implement in CAD models. A further benefit provided by lattice structures, one which is examined in this work, is their ability to absorb large amounts of deformation energy in a predictable manner, which is of great importance in the design of packaging materials and personal protective equipment (PPE) such as armour.

There are several variables in lattice structure design that affect their mechanical properties and deformation behaviour. The feature that has received most attention to date is the relative density, or volume fraction, of the lattice; see, for instance, the studies of Yan et al. [8,9] and Gümrük et al. [10]. This is unsurprising, since the relationships between volume fraction and the usual properties of interest, such as the modulus and strength of the lattice, are well established and have been verified for another, closely related, structure type; foams [11–13]. Other lattice design variables include the size and geometry of the tessellating unit cell. Only a handful of lattice cell types have been manufactured by AM and mechanically tested so far, most coming from the family of strut-based cells, such as the body-centred-cubic (BCC), the face-centred-cubic (FCC) and several reinforced versions of these [5,10,14–16].

There exists another family of geometries which have great potential as AM lattices; the triply periodic minimal surfaces (TPMS). Of these, only the Shoen gyroid has been examined in detail; experimentally by Yan et al. [3,8,9,17] and theoretically by Khaderi et al. [18]. One form of the gyroid lattice known as the double gyroid (DG) was recently identified as having high stiffness and low maximum von Mises stress compared to a variety of other cell types [19], making it particularly suitable for use in lightweight components. Furthermore, Aremu et al. [19] noted that the DG lattice, unlike several other lattice types, possesses axisymmetric stiffness, again making it a good candidate for applications where the exact nature and direction of the loads are not fully known or if they are subject to large uncertainties. The theoretical study by

* Corresponding author.
E-mail address: ian.maskery@nottingham.ac.uk (I. Maskery).

http://dx.doi.org/10.1016/j.addma.2017.04.003

Kapfer et al. [20] indicated that the DG lattice possessed superior mechanical properties compared to its network phase equivalent. In a novel demonstration of the DG structure's suitability for AM, Qin et al. [21] recently examined 3D graphene assemblies based on the DG architecture, deriving scaling laws for their mechanical performance. More information regarding the gyroid geometry and naming scheme is provided in Section 2.1.

Al-Si10-Mg belongs to a family of high strength aluminium alloys known for their good castability, corrosion resistance and ability to be strengthened by artificial ageing [22]. These alloys are used throughout the aerospace and automotive sectors, where the weights of all components, even the smallest and lightest, are scrutinised as they cumulatively affect the performance of the vehicle in which they reside, as well as the associated running costs and greenhouse gas emissions. Al-Si10-Mg is therefore a good material for investigations with AM lattices, as the demand for lightweight components in high strength alloys is already established. A post-manufacture heat treatment was applied to the lattice structures because it was previously observed to significantly alter the microstructure and mechanical properties of selectively laser melted Al-Si10-Mg [23,24], enhancing its ductility at the expense of reduced strength. Another relevant result comes from Maskery et al. [25], who applied the same heat treatment to strut-based Al-Si10-Mg lattice structures, finding that it improved their ability to absorb energy under compressive deformation compared to as-built structures.

In this paper, we address the relationship between structural performance and cell size in AM lattices, which to date has received little attention but is an important factor in AM lattice design. We go on to investigate the effect of an easily implementable heat treatment on lattice deformation, before quantifying and comparing the energy absorption of heat treated and as-built specimens. Following this introduction, the details of lattice design, production, testing and heat treatment are given, followed by the experimental results and discussion. Conclusions are provided in the final section.

2. Experimental details

2.1. Gyroid lattice design

The gyroid belongs to the family of triply periodic minimal surfaces (TPMS), a subset of the larger class of constant mean curvature (CMC) surfaces. In particular, TPMS are categorised by their zero mean curvature at every point.

TPMS equations describe 3D surfaces which, for the purpose of AM, can be taken as the boundary between void and solid material. Matrix phase gyroid structures with arbitrary numbers of cells and volume fractions can be generated by finding the $U=0$ isosurface of the equation

$$U = (\cos(k_x x)\sin(k_y y) + \cos(k_y y)\sin(k_z z) + \cos(k_z z)\sin(k_x x))^2 - t^2, \quad (1)$$

where k_i are the TPMS function periodicities, defined by

$$k_i = 2\pi\frac{n_i}{L_i} \text{ (with } \quad i = x, y, z), \quad (2)$$

n_i are the numbers of cell repetitions in x, y and z, and L_i are the absolute sizes of the structure in those dimensions.

Matrix phase lattices comprise a wall of solid material bounded by two unconnected void regions. These are distinct from network phase structures, which contain only one solid and one void region. This is illustrated in Fig. 1. In this paper, we will adopt the convention of referring to the matrix phase gyroid lattice as the double gyroid (DG).

In Eq. (1), t effectively controls the thickness of the cell walls, and thus also the volume fraction, ρ^*, of the resulting lattice structure. The relationship between t and ρ^* is unique for each TPMS cell type. For the DG lattice, we found this can be approximated reasonably well (in the range $0.1 \leq \rho^* \leq 0.9$) with the linear equation $\rho^* = 0.675t - 0.012$, though, to ensure the DG lattices in this paper possessed exactly the desired volume fraction, we employed a higher order polynomial form of $\rho^*(t)$.

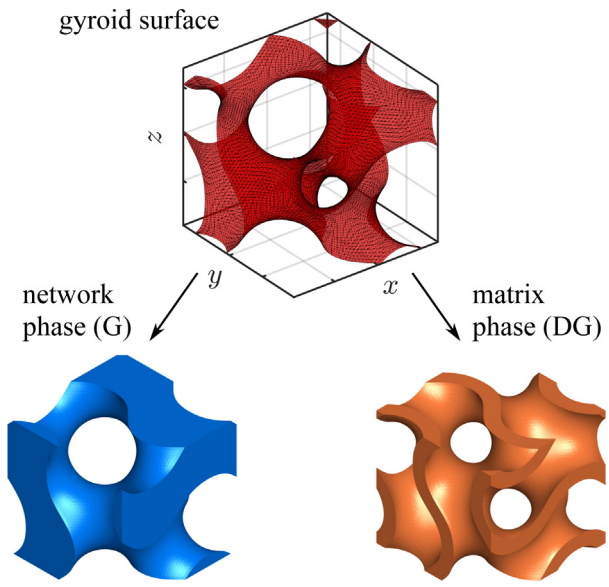

Fig. 1. The TPMS gyroid surface (above) provides the network and matrix phase cells for AM (below).

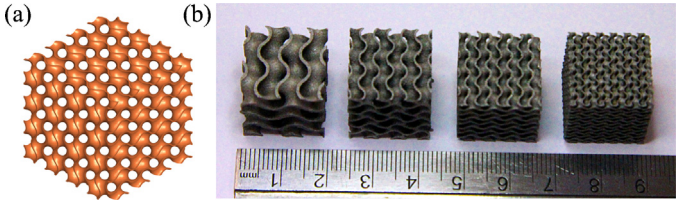

Fig. 2. CAD representation of the DG lattice (a) and photographs of SLM manufactured specimens (b). The specimens in (b), from left to right, contain cells of size 9, 6, 4.5 and 3 mm.

2.2. Selective laser melting of double gyroid lattice specimens

Double gyroid lattice specimens composed of Al-Si10-Mg were fabricated using a Renishaw AM250 selective laser melting (SLM) machine. The laser power was 200 W and a meandering scan pattern with 130 μm hatch spacing was used. The laser point distance and exposure time were 80 μm and 140 μs, respectively. The Al-Si10-Mg powder was deposited in 25 μm layers prior to each laser scan and the build platform was held at 180 °C during specimen production. Photographs of manufactured DG lattice structures are provided in Fig. 2, alongside a CAD representation. The range of DG lattice unit cell sizes was 3, 4.5, 6 and 9 mm, which were chosen to provide integer periodicities in the 18 mm specimens. These specifications, along with the total number of lattice cells and the wall thickness for each specimen, are provided in Table 1. The volume fraction in each case was 0.22, which was obtained using $t = 0.3409$ in Eq. (1).

2.3. SLM material and lattice characterisation

Uniaxial compression testing of the DG lattice specimens was conducted using an Instron 5969 universal testing machine with a 50 kN load cell. The loading direction was equivalent to the SLM building direction. The compressive deformation rate was

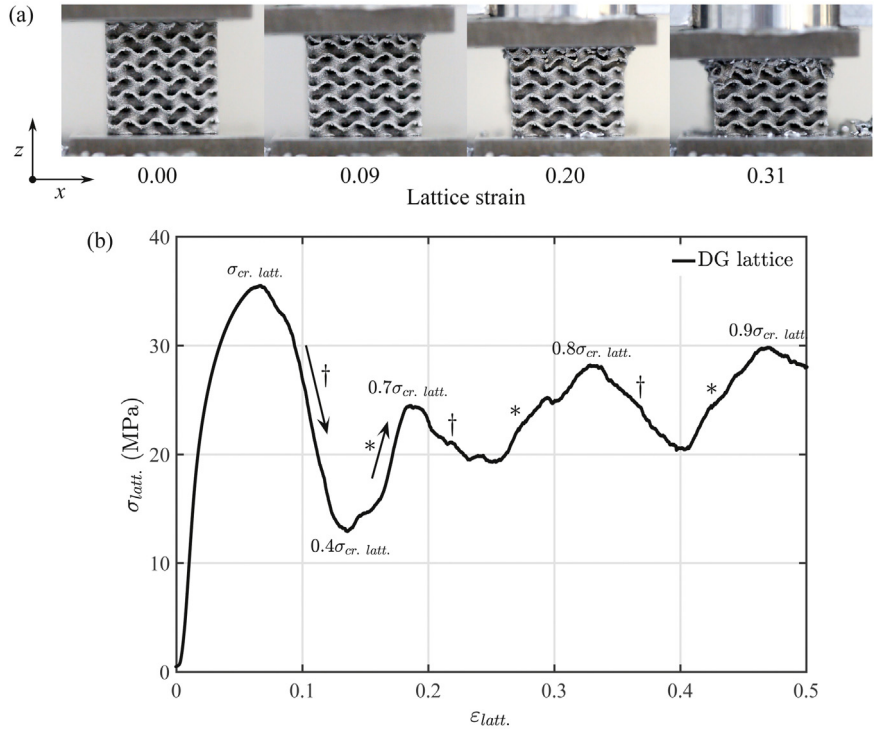

Fig. 3. Successive layer collapse and densification of DG lattices with 4.5 mm cells; video frames during compression (a) and resulting stress-strain curve (b).

Table 1
Specifications of the DG lattices used in this study.

Cell size (mm)	Lattice configuration	No. of cells	Cell wall thickness (mm)
3	6 × 6 × 6	216	0.33
4.5	4 × 4 × 4	64	0.50
6	3 × 3 × 3	27	0.66
9	2 × 2 × 2	8	1.00

Table 2
Elastic modulus, ultimate tensile strength and strain-to-failure of as-built and heat treated SLM Al-Si10-Mg.

	As-built	Heat treated
E (GPa)	81 ± 2	80 ± 2
σ_{UTS} (MPa)	330 ± 10	292 ± 4
ε_{UTS} (%)	1.4 ± 0.3	3.9 ± 0.5

9×10^{-3} mm/s. Deformation data were collected using a linear variable differential transformer (LVDT), while the collapse of each specimen was recorded by video with a frame rate of 50 Hz. This provided information regarding the failure modes of the lattice structures. For the as-built (i.e. not heat treated) specimens, the compression tests were ended after the first major structural collapse, usually signified by the brittle fracture of the specimen into multiple pieces. Otherwise, the compression tests were terminated at a strain of 50%.

The mechanical properties of bulk SLM Al-Si10-Mg were determined by a series of uniaxial tension tests in accordance with ASTM standard E8/E8M [26]. The ram speed was 8.3×10^{-3} mm/s. A video gauge was used to collect the strain data from the tensile specimens, their surfaces having been given a 'spatter' coating of paint to facilitate video point tracking. These tests were conducted with an Instron 5581 universal testing machine with a 50 kN load cell.

Scanning electron microscopy (SEM) was used to examine the fractured struts and walls of some DG lattices. This was conducted with a Hitachi TM3030 microscope using an accelerating voltage of 15 kV.

2.4. Heat treatment of SLM Al-Si10-Mg

Following mechanical testing in their as-built condition, DG lattice structures with 3 mm unit cells were given a post-manufacture heat treatment. This comprised a solution treatment for 1 h at 520 °C followed by a water quench and artificial ageing for 6 h at 160 °C. This treatment was previously found by Aboulkhair et al. [27] to modify the microstructure of SLM Al-Si10-Mg and reduce its hardness by nearly 30% compared to as-built condition. For a discussion of the effect of the heat treatment on the microstructure and stress–strain behaviour of SLM Al-Si10-Mg, the reader is directed to the works of Aboulkhair et al. [23] and Maskery et al. [25]. In Table 2 we present the mechanical properties of as-built and heat treated SLM Al-Si10-Mg that are most relevant to this work. Heat treatment reduces the ultimate tensile strength (UTS) of the material by (12 ± 3)%, whilst significantly enhancing its ductility.

3. Results and discussion

3.1. Double gyroid lattice failure modes

As-built DG lattice structures exhibited a variety of compressive failure modes. The first is represented in Fig. 3(a). This was the successive collapse of cells in planes perpendicular to the manufacturing and loading direction (z). This occurred in only a small number of examined specimens, and only for those composed of 4.5 mm and 6 mm cells. This type of structural failure gave rise to stress–strain curves such as that in Fig. 3(b), where the strength was repeatedly lost († symbol) and recovered (* symbol) as each layer collapsed and was compressed into the one below. The structure grew stronger after the densification of each layer, recovering up to ~90% of the initial crushing strength, $\sigma_{cr.\ latt.}$, before reaching 50% strain.

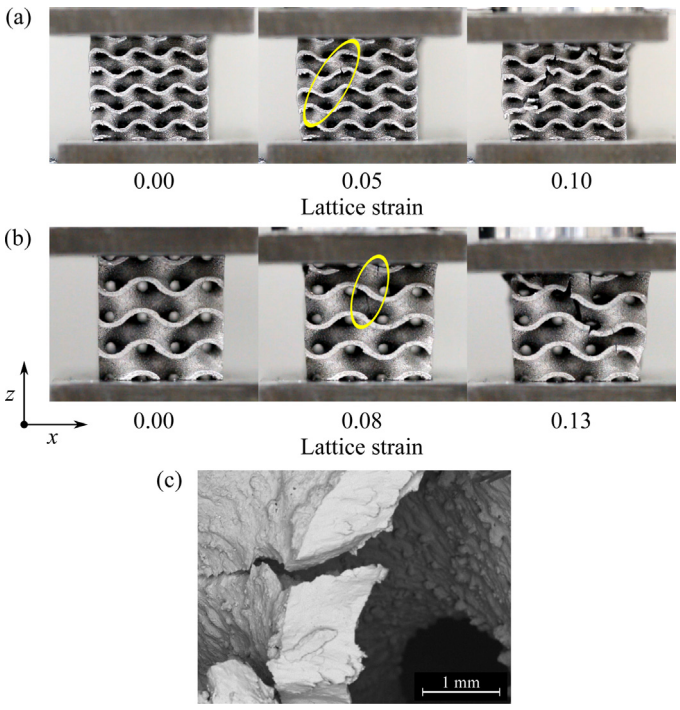

Fig. 4. Low strain crack initiation and propagation in DG lattices with 6 mm cells (a) and 9 mm cells (b). The fracture surface in (c) occurred in a lattice with 9 mm cells.

The second type of failure observed in DG structures occurred for those composed of larger cells, 6 mm and 9 mm, only. It was also due to brittle fracturing of the cell walls, and was characterised by the propagation of a crack, or cracks, through the lattice, often with the main component of the direction of crack propagation parallel to the applied load – see Fig. 4(a) and (b). The complexity of the DG geometry makes identification of the crack initiation site troublesome, though it is most likely to originate at a pre-existing defect, such as an internal pore of surface irregularity. The path of the cracks through the DG structure was also hard to determine; the specimens were fractured into many small pieces, so visual analysis after failure was uninformative. The micrograph shown in Fig. 4(c) makes it clear that a crack can fork perpendicularly to its direction of propagation through the walls of the DG cells, implying that crack propagation through the structure is likely tortuous.

The third mode of failure seen in DG structures was diagonal shear. This occurred almost exclusively in the DG lattices with the smallest, 3 mm, cells, as shown in Fig. 5. This resulted in stress–strain curves such as that shown in Fig. 6 – an initial loss of 50% strength, followed by relatively uniform strengthening through densification, up to ~90% of $\sigma_{cr.\,latt.}$ just below 50% strain, as the upper and lower parts of the structure were forced together. The formation of a diagonal shear band 45° to the loading direction has previously been seen in other lattice types [28,29,25] made by SLM.

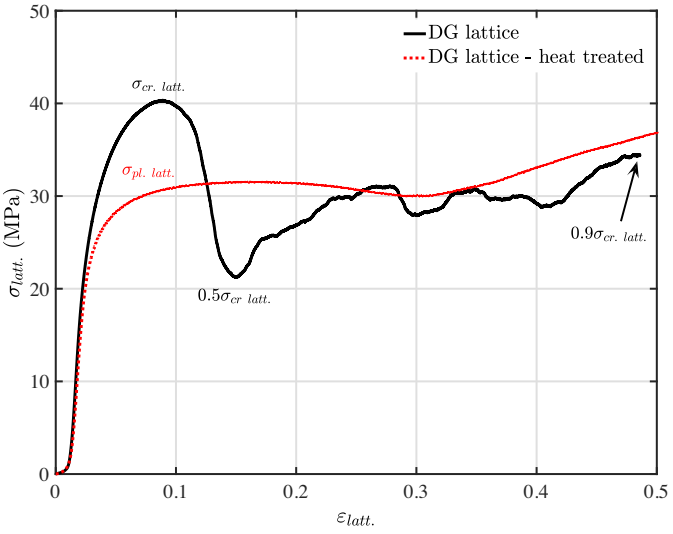

Fig. 6. Stress–strain curves of as-built and heat treated DG lattices with 3 mm cells.

It is clear from Figs. 3, 4 and 5 that the compressive failure mode of the DG lattice is related to the size of its constituent cells. In general, specimens with 9 mm cells, which had only 2 repeating cells in each orthogonal direction, exhibited very different crushing behaviour than those with 3 mm cells, which had 6 cells in each direction.

3.2. The effect of heat treatment upon compressive deformation

Because of their favourable deformation behaviour compared to the other types, DG lattices with 3 mm cells were chosen to examine the effect of a post-manufacture heat treatment (as outlined in Section 2.4). Following heat treatment, the deformation of DG lattices with 3 mm cells was seen to change significantly. None of the heat treated lattices exhibited low-strain brittle failure. Their stress–strain curves (see Fig. 6) included the long plateaux more closely resembling the ideal cellular solid deformation depicted by Gibson and Ashby [11]. This transformation to a relatively flat stress-strain curve from one featuring unpredictable weakening due to localised brittle collapse is a significant outcome of this work. It suggests a route by which the scaling laws and design rules developed by Gibson and Ashby [11] and others, which generally assume an ideal plastic plateau for the purpose of energy absorption, may be made relevant to cellular structures made by SLM.

Also evident in Fig. 6 is the effect of the heat treatment on the crushing or collapse strength of the structures, which was reduced by ~25% compared to the as-built lattices; the effect is around twice as large as the reduction in UTS of the solid tensile specimens described in Section 2.4. However, the heat treated stress-strain curve of Fig. 6 also shows some non-ideal behaviour; decreasing then increasing strength above strain levels of around 20%. These

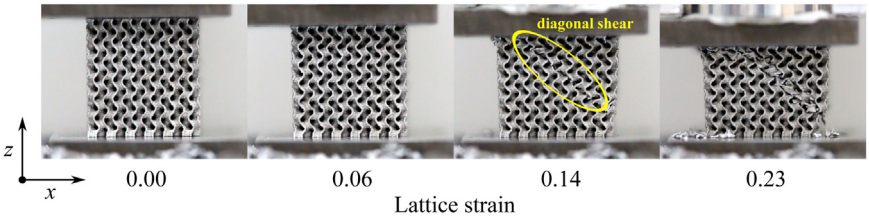

Fig. 5. Diagonal shear failure in DG lattices with 3 mm cells. (Note that the loading direction in this figure is the same as shown in Figs. 3 and 4; the orientation of the cellular walls is different because the compressive test was filmed from an angle orthogonal to the others. Fig. 1 shows that the DG lattice does not possess rotational symmetry around the *z* axis.)

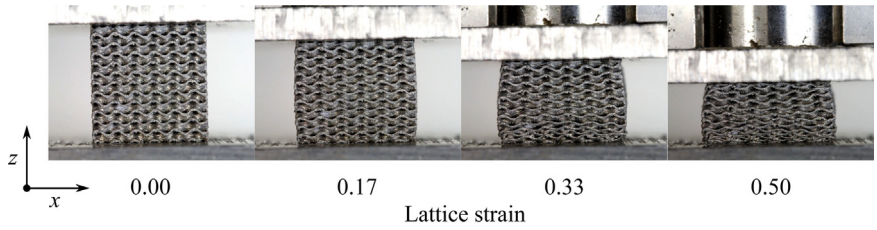

Fig. 7. Compressive deformation of heat treated DG lattices with 3 mm cells.

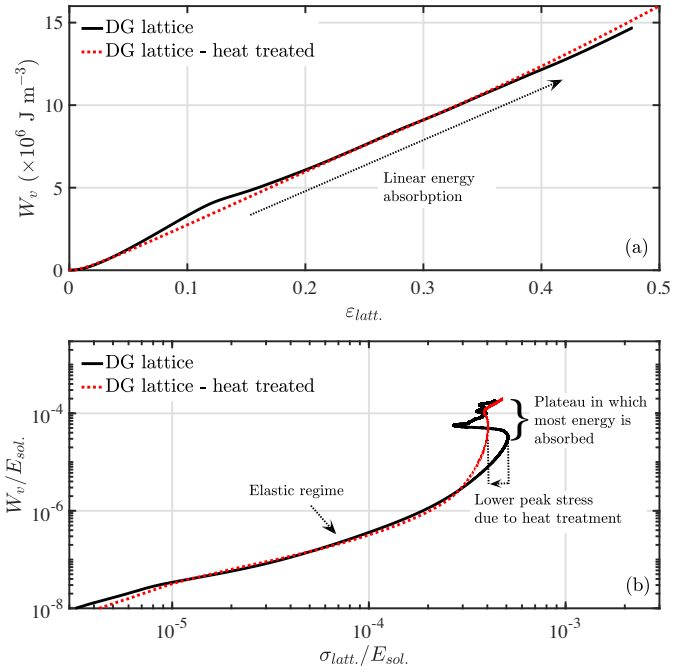

Fig. 8. Energy absorption per unit volume, W_v, of as-built and heat treated DG lattices with 3 mm cells. In (b) W_v and $\sigma_{latt.}$ are normalised by the modulus of the cell wall material, E_{sol}.

features were likely caused by competing mechanisms. First, constrained deformation of the lattices due friction at the anvil surfaces led to localised buckling, and therefore weakening of the structures. This is evident in the central bulging, or barrelling, of the structures, as seen in Fig. 7. Second, there is the onset of local densification above ~30% strain, supporting evidence for which can be seen in Fig. 7, where it is clear that cells toward the bottom of the structure have undergone at least partial collapse prior to those above.

3.3. Lattice energy absorption

In Fig. 8 are presented the energy absorption of as-built and heat treated DG lattices structures in two common ways. Fig. 8(a) shows cumulative energy absorption per unit volume, W_v, plotted against the effective lattice strain. From this we can see that as-built and heat treated DG lattices absorb energy almost linearly with strain, which is consistent with the pre-densification behaviour seen for Al-Si10-Mg BCC lattices also made by SLM [25]. The total energy absorbed by heat treated DG lattices up to 50% strain was 16×10^6 J m^{-3}; this is close to three times the energy absorbed by the previously examined BCC lattices [25] (which had the same volume fraction as the DG lattices examined here).

In Fig. 8(b), W_v is plotted against $\sigma_{latt.}$, both normalised by the modulus of the cell wall material, $E_{sol.}$, as determined from the uniaxial tests described in Sections 2.3 and 2.4. This form of energy absorption diagram was used by Gibson and Ashby in their influential discussions of cellular solids [11], and is useful in allowing a designer to choose a cellular structure which provides the most appropriate absorption profile for a given application. When populated with curves representing a range of lattice variables (for example, lattices with different cell type, volume fraction, material or post-manufacture treatment), this diagram can specify the structure offering maximal energy absorption without exceeding a maximum permitted stress, which is exactly the problem underpinning the design of packaging materials and PPE. Thus, we can see from Fig. 8(b) that the heat treated DG lattice is superior to the as-built lattice, in that it provides the same total energy absorption but with a significantly lower peak stress prior to energy absorption in the plateau region. The normalised peak stresses of the as-built and heat treated DG lattices were 5×10^{-4} and 4×10^{-4}, respectively.

4. Conclusions

Our investigation has revealed that cell size plays an important role in determining the failure mechanism of metal AM lattices. To avoid low-strain structural failure due to localised fracture and crack propagation, one should choose a small cell size. In practice however, this may pose a problem, because the smallest features of the cells, be they struts or continuous walls, as examined here, clearly must not approach the manufacturing resolution of the AM platform in question, otherwise they will be reproduced inaccurately. This design-for-AM problem is undoubtedly worthy of further investigation.

We also demonstrated that the deformation process of SLM aluminium lattices can be improved by a readily applied post-manufacture heat treatment. The heat treatment used here prevented the formation of a diagonal shear band in DG lattice structures, giving rise to a plateau in the stress-strain curve usually associated with ideal deformation in cellular solids. The heat treated lattices absorbed the same amount of energy under compressive deformation as the as-built lattices, but they did so experiencing a significantly lower peak stress. The benefit of a relatively flat stress plateau can be most easily appreciated considering the example of PPE such as body armour, where the energy of an incident blast wave or projectile must be absorbed uniformly and predictably to reduce the risk of harm to the user. Therefore, we can recommend that for applications involving the absorption of deformation energy below a predefined stress threshold, aluminium SLM lattices should be heat treated as a matter of course.

Finally, we found that the specific energy absorbed by heat treated DG lattices up to 50% compressive strain was nearly three times that absorbed by comparable BCC lattices in a previous study [25]. This makes a strong case for the use of DG lattices, and perhaps other TPMS lattice types too, in lightweight, energy absorbing applications.

Acknowledgments

This work was supported by the Engineering and Physical Sciences Research Council [grant number EP/I033335/2] and also by

Innovate UK [project number 102665]. Thanks to Mark East, Mark Hardy and Joe White, technicians of the Centre for Additive Manufacturing, and also to Jason Greaves, who assisted with sample compression measurements.

References

[1] D. Brackett, I. Ashcroft, R. Wildman, R. Hague, An error diffusion based method to generate functionally graded cellular structures, Comput. Struct. 138 (0) (2014) 102–111.
[2] J. Brennan-Craddock, D. Brackett, R. Wildman, R. Hague, The design of impact absorbing structures for additive manufacture, J. Phys.: Conf. Ser. 382 (1) (2012) 012042.
[3] C. Yan, L. Hao, A. Hussein, P. Young, J. Huang, W. Zhu, Microstructure and mechanical properties of aluminium alloy cellular lattice structures manufactured by direct metal laser sintering, Mater. Sci. Eng. A – Struct. 628 (0) (2015) 238–246.
[4] K. Ushijima, W.J. Cantrell, R.A.W. Mines, S. Tsopanos, M. Smith, An investigation into the compressive properties of stainless steel micro-lattice structures, J. Sandw. Struct. Mater. 13 (2011) 303–329.
[5] B. Gorny, T. Niendorf, J. Lackmann, M. Thoene, T. Troester, H. Maier, In situ characterization of the deformation and failure behavior of non-stochastic porous structures processed by selective laser melting, Mater. Sci. Eng. A – Struct. 528 (2011) 7962–7967.
[6] G.W. Kooistra, V.S. Deshpande, H.N. Wadley, Compressive behavior of age hardenable tetrahedral lattice truss structures made from aluminium, Acta Mater. 52 (2004) 4229–4237.
[7] N.A. Fleck, V.S. Deshpande, M.F. Ashby, Micro-architectured materials: past, present and future, Proc. R. Soc. A 466 (2010) 2495–2516.
[8] C. Yan, L. Hao, A. Hussein, P. Young, D. Raymont, Advanced lightweight 316L stainless steel cellular lattice structures fabricated via selective laser melting, Mater. Des. 55 (2014) 533–541.
[9] C. Yan, L. Hao, A. Hussein, S.L. Bubb, P. Young, D. Raymont, Evaluation of light-weight AlSi10Mg periodic cellular lattice structures fabricated via direct metal laser sintering, J. Mater. Process. Technol. 214 (2014) 856–864.
[10] R. Gümrük, R. Mines, S. Karadeniz, Static mechanical behaviours of stainless steel micro-lattice structures under different loading conditions, Mater. Sci. Eng. A – Struct. 586 (0) (2013) 392–406.
[11] L. Gibson, M. Ashby, Cellular Solids: Structure and Properties, Cambridge University Press, 1997.
[12] M. Ashby, A. Evans, N. Fleck, L. Gibson, L. Hutchinson, H. Wadley, Metal Foam: A Design Guide, Butterworth-Heinemann, 2000.
[13] U. Ramamurty, A. Paul, Variability in mechanical properties of a metal foam, Acta Mater. 52 (2004) 869–876.
[14] I. Maskery, A. Hussey, A. Panesar, A. Aremu, C. Tuck, I. Ashcroft, R. Hague, An investigation into reinforced and functionally graded lattice structures, J. Cell Plast. 53 (2) (2017) 151–165.
[15] R. Gümrük, R. Mines, Compressive behaviour of stainless steel micro-lattice structures, Int. J. Mech. Sci. 68 (0) (2013) 125–139.
[16] S. Merkt, C. Hinke, J. Bültmann, M. Brandt, Y.M. Xie, Mechanical response of TiAl6V4 lattice structures manufactured by selective laser melting in quasistatic and dynamic compression tests, J. Laser. Appl. 27 (S1) (2015).
[17] C. Yan, L. Hao, A. Hussein, D. Raymont, Evaluations of cellular lattice structures manufactured using selective laser melting, Int. J. Mach. Tool Manuf. 62 (2012) 32.
[18] S. Khaderi, V. Deshpande, N. Fleck, The stiffness and strength of the gyroid lattice, Int. J. Solids Struct. 51 (2324) (2014) 3866–3877.
[19] A. Aremu, I. Maskery, C. Tuck, I. Ashcroft, R. Wildman, R. Hague, A comparative finite element study of cubic unit cells for selective laser melting, Solid Freeform Fabrication Symposium (2014).
[20] S.C. Kapfer, S.T. Hyde, K. Mecke, C.H. Arns, G.E. Schröder-Turk, Minimal surface scaffold designs for tissue engineering, Biomaterials 32 (29) (2011) 6875–6882.
[21] Z. Qin, G.S. Jung, M.J. Kang, M.J. Buehler, The mechanics and design of a lightweight three-dimensional graphene assembly, Sci. Adv. 3 (2017) e1601536.
[22] J. Kaufman, E. Rooy, Aluminum Alloy Castings: Properties, Processes, and Applications, AFS, 2004.
[23] N.T. Aboulkhair, I. Maskery, C. Tuck, I. Ashcroft, N.M. Everitt, The microstructure and mechanical properties of selectively laser melted AlSi10Mg: the effect of a conventional T6-like heat treatment, Mater. Sci. Eng. A – Struct. 667 (2016) 139–146.
[24] N.T. Aboulkhair, I. Maskery, C. Tuck, I. Ashcroft, N.M. Everitt, Improving the fatigue behaviour of a selectively laser melted aluminium alloy: influence of heat treatment and surface quality, Mater. Des. 104 (2016) 174–182.
[25] I. Maskery, N. Aboulkhair, A. Aremu, C. Tuck, I. Ashcroft, R. Wildman, R. Hague, A mechanical property evaluation of graded density Al-Si10-Mg lattice structures manufactured by selective laser melting, Mater. Sci. Eng. A – Struct. 670 (2016) 264–274.
[26] E8/E8M – 15 Standard Test Methods for Tension Testing of Metallic Materials, ASTM International, 2015.
[27] N. Aboulkhair, C. Tuck, I. Ashcroft, I. Maskery, N. Everitt, On the precipitation hardening of selective laser melted AlSi10Mg, Metal. Mater. Trans. A 46 (2015) 3337.
[28] R. Hasan, R.A. Mines, E. Shen, S. Tsopanos, W. Cantwell, Comparison on compressive behaviour of aluminium honeycomb and titanium alloy micro lattice blocks, Key Eng. Mater. 462 (2011) 212–218.
[29] C. Qiu, S. Yue, N.J. Adkins, M. Ward, H. Hassanin, P.D. Lee, P.J. Withers, M.M. Attallah, Influence of processing conditions on strut structure and compressive properties of cellular lattice structures fabricated by selective laser melting, Mater. Sci. Eng. A – Struct. 628 (2015) 188–197.